

# EXPERIMENTAL REALIZATION OF ENTANGLED QUTRITS FOR QUANTUM COMMUNICATION

R. Thew<sup>1</sup> A. Acín<sup>1,2</sup>, H. Zbinden<sup>1</sup> and N. Gisin<sup>1</sup>

<sup>1</sup>*Group of Applied Physics, University of Geneva, 1211 Geneva 4, Switzerland*  
*and*

<sup>2</sup>*Institut de Ciències Fotòniques, Jordi Girona 29, 08034 Barcelona, Spain*

We have experimentally realized a technique to generate, control and measure entangled qutrits, 3-dimensional quantum systems. This scheme uses spontaneous parametric down converted photons and unbalanced 3-arm fiber optic interferometers in a scheme analogous to the Franson interferometric arrangement for qubits. The results reveal a source capable of generating maximally entangled states with a net state fidelity,  $F = 0.985 \pm 0.018$ . Further the control over the system reveals a high, net, 2-photon interference fringe visibility,  $V = 0.919 \pm 0.026$ . This has all been done at telecom wavelengths thus facilitating the advancement towards long distance higher dimensional quantum communication.

*Keywords:* qutrit, entanglement, quantum communication

## 1. Introduction

Quantum information science is now a well recognized branch of science in its own right, dealing with a diverse range of theoretical and practical issues related to quantum computing and quantum communication [1]. At the heart of this field has been the idea of the Qubit, simply, a two dimensional quantum system. Theory and experiment, especially within the optics community, has advanced rapidly, both from a fundamental as well as applied perspective. Already we have quantum key distribution (QKD) [2] as the first quantum technology to be taken into the public domain. One question that has received significant theoretical interest in the past few years is - what can we do with high dimensional systems?

There have recently been several proposals for quantum communication protocols involving higher dimensional states, specifically qutrits (three dimensional quantum systems). In some cases these have advantages over qubit protocols, like increased robustness against noise in quantum key distribution schemes [3, 4, 5]. However, the more interesting cases are those where it is more efficient to have a system encoded using qutrits than qubits, specifically for

the solution to the Byzantine Agreement Problem [6] or for Quantum Coin Tossing [7]. As such we would like an efficient source of entangled qutrits to take advantage of these protocols. Also, if we can approach these qutrit and higher dimensional systems with the same positive perspective that has been accorded the qubit then what we have are larger quantum system in which to perform even more complex quantum protocols.

There are two possible approaches that can be taken if we want to investigate higher dimensional systems: use multiple (more than 2) entangled qubit systems [8, 9, 10, 11, 12]; or increase the dimensions of the fundamental elements. If we increase the dimensions of the elements, the simplest place to start to answer some of the questions experimentally is with qutrits. Recently there have been some advances to this end: the generation of qutrits using bi-photons [13]; and two schemes generating entangled qudits,  $d$ -level quantum systems. The first, using the orbital angular momentum of light, have specifically shown their scheme setup to analyze qutrits [14], while the second uses a pulsed, mode-locked, laser to generate time-bin qudits where they have shown entanglement up to  $d = 11$  [15].

The scheme we use is based on energy-time entanglement and is analogous to the Franson-type interferometric arrangement for photonic qubits [16]. A similar idea for such an experiment had previously been proposed however only preliminary experimental results followed [17, 18, 19]. In this article we introduce an experimental setup where we can generate, manipulate and measure entangled qutrits. We first detail our experimental set-up and show how this corresponds to the theoretical description of qutrits before deriving two different means of analyzing the output of the system.

## 2. Experimental Set-up

Consider the experimental schematic of Fig.1. We are using a continuous wave (CW) external grating diode laser (Toptica DL100) at 657 nm incident on a Periodically Poled Lithium Niobate (PPLN) waveguide where spontaneous Parametric Down Conversion (PDC) produces degenerate, collinear, energy-time entangled photon pairs at 1314 nm. The PPLN waveguide has proven to be a highly efficient and stable source of PDC photons [20] which allows one to use a simple laser diode instead of a large, complex, and expensive laser system often required when using standard non-linear crystals. The photon pairs are coupled into a monomode optical fiber before passing through a fiber beam splitter (BS) which separates the photon pairs and sends them to one of the two all-fiber Michelson interferometers.

Each of the interferometers consist of a 6-port symmetric coupler [21]  $T_A$  and  $T_B$ , also known as tritters. These are the three dimensional extension to a standard beam splitter or 50/50 fiber coupler. Ideally they take an input signal in any of the three inputs and distribute it with equal probability in the three output ports. Thus ideally we would like a 33/33/33 fiber coupler. The splitting ratios have been measured for both of these and we find that the deviation from this ideal value is around 5%. Even a variation of 10% would only correspond to a reduction in state fidelity of less than 1%. The fidelity is not the most sensitive measure [22] but this symmetry is crucial in simplifying the analysis of the system as we will see momentarily.

When the photons enter the interferometers via the tritters  $T_A$  and  $T_B$ , they have a choice of three paths. The three possibilities hence define the qutrit space. We encode these possible paths via the path-lengths, ie. short, medium, long, or 0,1,2, as labelled. We define the three

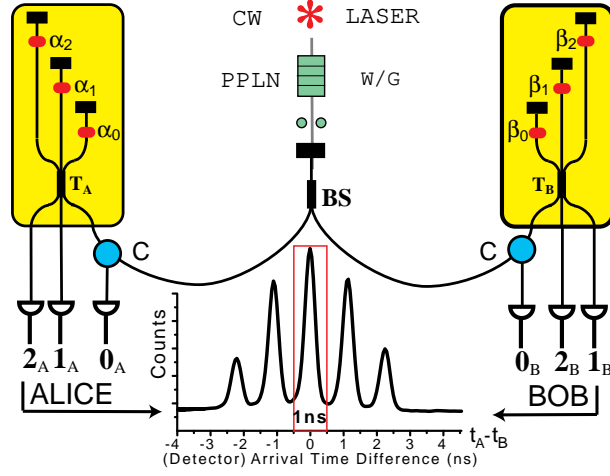


Fig. 1. Schematic of experiment for generation and analysis of entangled qutrits: Down-Converted photon pairs at telecom wavelengths combined with unbalanced three path interferometers are used to generate and analyze energy-time entangled qutrits.

different path lengths such that the path-length differences in both interferometers are the same, within the coherence length of the PDC photons. More formally we require that the path lengths satisfy,

$$l^A - m^A \approx m^A - s^A \approx l^B - m^B \approx m^B - s^B \quad (1)$$

where, for example,  $m^A$  denotes the length of fibre for the medium arm in Alice's interferometer. The path length differences define the separation of the five peaks in the time-of-arrival histogram inset into Fig.1, which has been chosen to be  $\Delta\tau = 1.2 \text{ ns}$ . Although we are encoding our qutrits with time-bins we also need to be careful with the polarization state of the photons. Inside the fiber interferometer the polarization can vary and hence one could possibly determine which path was taken by the photon. To overcome this problem we use Faraday Mirrors at the ends of these fiber arms so that when a photon returns to the tritter its polarization is always orthogonal to when it entered, *regardless of the path taken*, thus reducing the which-path information. Any which-path information could in turn diminish the quality of the entanglement resource.

When the photons leave the interferometers there are nine possible detection combinations that can be observed between each of Alice and Bob's three detectors. We can put optical Circulators (C) on one input port of each interferometer so we can detect all of these. As well as this there are nine different path combinations through the two interferometers for each detection combination. These are represented in the time-of-arrival histogram inset in Fig.1. The two outside peaks correspond to a difference in the arrival time of the photon pairs of  $\pm 2\Delta\tau$ , where one photon passes through a short arm and the other passes through a long arm. The next two lateral peaks, either side of the central peak, correspond to photons passing through the short and medium *or* the medium and long arms and arriving with  $\pm\Delta\tau$  and thus being on the left or right of the central peak. Finally, the central peak corresponds to

where the photons take the same path in each interferometer, short-short, medium-medium, or long-long and arrive with no time difference.

We can only discuss these events in this manner under the following circumstances: the coherence length of the PDC photons is much smaller than the path-length difference in the interferometers (40 nm  $\ll$  24 cm) so that no single photon interference effects are observed in passing the interferometers; the coherence length of the pump laser is much greater than these path-length differences (48 cm  $\ll$   $\mathcal{O}(100\text{ m})$ ) so that we have no timing information as to the creation time of the photon pair and hence which path was taken before detection. If we do this we can then describe the experiment as follows. We use energy-time correlated photon pairs distributed to two tritters as our source of qutrits. We claim, that these are maximally entangled qutrits due to the symmetry of the coupling ratio of the tritters. The different path-lengths in the interferometers defines a transform basis and provides a means of individually addressing the two free phases with local phase operations. The photons leaving the interferometers via their respective tritters and then being detected can be viewed as a projective measurement onto the entangled qutrit state space.

Therefore, with these assumptions we can define three orthogonal, maximally entangled, qutrit states for the three different possible coincidence detection combinations.

$$|\psi_{00}\rangle = \frac{1}{\sqrt{27}}[|00\rangle + e^{i(\alpha_1 - \alpha_0 + \beta_1 - \beta_0 + t)}|11\rangle + e^{i(\alpha_2 - \alpha_0 + \beta_2 - \beta_0 + t)}|22\rangle] \quad (2)$$

$$|\psi_{01}\rangle = \frac{1}{\sqrt{27}}[|00\rangle + e^{i(\alpha_1 - \alpha_0 + \beta_1 - \beta_0)}|11\rangle + e^{i(\alpha_2 - \alpha_0 + \beta_2 - \beta_0 - t)}|22\rangle] \quad (3)$$

$$|\psi_{02}\rangle = \frac{1}{\sqrt{27}}[|00\rangle + e^{i(\alpha_1 - \alpha_0 + \beta_1 - \beta_0 - t)}|11\rangle + e^{i(\alpha_2 - \alpha_0 + \beta_2 - \beta_0)}|22\rangle]. \quad (4)$$

Here  $|\psi_{01}\rangle$  describes the state, determined by the interferometer paths and phase settings, that leads to a coincidence detection between Alice's detector 0 and Bob's detector 1.  $|11\rangle = |1\rangle_A \otimes |1\rangle_B$  corresponds to the photon taking the medium path in both interferometers. The phases that can be applied in each arm of the interferometers are denoted by  $\alpha_j, \beta_j$ . We have also introduced the factor  $t = 2\pi/3$  which is the phase obtained when a photon changes ports in the tritters, analogous to the  $\pi/2$  phase obtained upon reflection in normal 4-port beam-splitters. The previously mentioned symmetry ensures that the states satisfy,  $|\psi_{00}\rangle = |\psi_{11}\rangle = |\psi_{22}\rangle$ ,  $|\psi_{01}\rangle = |\psi_{12}\rangle = |\psi_{20}\rangle$ , and  $|\psi_{02}\rangle = |\psi_{10}\rangle = |\psi_{21}\rangle$ .

Qutrit QKD, as mentioned in the introduction, can provide a more robust key distribution scheme than with qubits. It also provides another means to formulate a description of this experimental arrangement that may be more intuitive. Alice prepares her qutrit in one of the three transpose bases with her interferometer, generating a superposition of the three (computational) basis states, and her choice of phase settings [3]. She will obtain a click at one of three detectors, her trit value. She sends the other, "prepared" photon to Bob. Bob makes a choice about which basis with his interferometer and phase settings defining one of his three transform basis choices. He receives a click at one of his three detectors, his trit value. If their bases agree then the results are correlated and they can share a secret key. We

are performing this experiment at  $1.3\ \mu\text{m}$  and this type of encoding has already been shown to provide a robust form of entanglement for long distance quantum communication [23, 24] hence there are very few restrictions in extending the current scheme to longer distances for protocols of this type.

For detection we are using a combination of Ge and InGaAs Avalanche Photo-Diodes (APDs). The Ge work in a passive mode at 1314 nm and have efficiencies,  $\eta_{Ge} \approx 10\%$ . We use these on one side, Alice's, to trigger the InGaAs detectors (idQuantique id200) on Bob's side which need to be used in a gated mode but have a higher quantum efficiency,  $\eta_{InGaAs} > 20\%$ , and better noise characteristics. We use a Time-To-Digital converter to process these detection events which generates the data corresponding to arrival time differences between the start (Alice) and the three different stops (Bob). For each of these start-stop combinations we obtain an histogram like the one inset between Alice and Bob's detectors in Fig.1. We select events occurring within temporal windows  $\Delta\tau_w = 1\ \text{ns}$  about these peaks. Events in each central peak of the three histograms corresponds to a projection onto one of the three states previously listed.

The other peaks here are not without interest. The first two lateral peaks project onto different subspaces within the entangled qutrit Hilbert space. Specifically, detecting events in these peaks projects onto states of the form,

$$|\psi_{00}^R\rangle = \frac{1}{\sqrt{27}}[|01\rangle + e^{i(\alpha_1 - \alpha_0 + \beta_2 - \beta_1 - t)}|12\rangle] \quad (5)$$

for the right peak where the photons arrive with a fixed time difference  $\Delta\tau = 1.2\ \text{ns}$ . But there are two possibilities and we cannot distinguish photons that took the short(0) path at Alice's and the medium(1) path at Bob's from those that took the medium(1) at Alice's and the long(2) at Bob's. The left peak corresponds to those states having an arrival time difference of  $-\Delta\tau$ , and these project onto states of the form

$$|\psi_{00}^L\rangle = \frac{1}{\sqrt{27}}[|10\rangle + e^{i(\alpha_2 - \alpha_1 + \beta_1 - \beta_0 - t)}|21\rangle]. \quad (6)$$

Both left and right states here are entangled and their form is suggestive of the type of states required for optimal quantum coin tossing [7]. We have the same symmetry for the other detectors, as previously shown for the states in the central peak, and again these results differ by factors of  $t$ . The outer two peaks,  $\pm 2\Delta\tau$  difference in arrival times, ie.  $|02\rangle$  and  $|20\rangle$ , have no interfering effects and hence can be used to monitor the count rate. All of these measurements, and also that of the noise, can be made simultaneously.

We commented that states corresponding to these lateral peaks were interesting but they are also useful in controlling and characterizing the entangled qutrits of the central peak. We will vary the phases in just one, Alice's, interferometer, thus, to simplify the theory we can think of Bob's interferometer as a reference and set all of these phase settings to zero,  $(\beta_0, \beta_1, \beta_2) = (0, 0, 0)$ . If we do this we find that the lateral peaks now have corresponding states of the form:

$$\begin{aligned} |\psi_{00}^R\rangle &= |01\rangle + e^{i(\Phi_{00}^R + t)}|12\rangle & : & \quad \Phi_{00}^R \equiv \alpha_1 - \alpha_0 + t \\ |\psi_{00}^L\rangle &= |10\rangle + e^{i(\Phi_{00}^L - t)}|21\rangle & : & \quad \Phi_{00}^L \equiv \alpha_2 - \alpha_1, \end{aligned} \quad (7)$$

and similarly for the other two. We can then rewrite the entangled qutrit state of Eq.(2) as

$$|\psi_{00}\rangle = \frac{1}{\sqrt{27}}[|00\rangle + e^{i\Phi_{00}^R}|11\rangle + e^{i(\Phi_{00}^R + \Phi_{00}^L)}|22\rangle]. \quad (8)$$

In fact all three different states can be written in this form with the phase shift of  $t$  within the definition of the phase of the lateral peaks. Thus, if we are trying to align the interferometers or determine some relative phases we can observe the various probabilities of coincidence in the associated peak of the time-of-arrival histogram to assist us. By observing the behavior of these lateral peaks we can control the relationship between the two phases.

In the interferometers we control the phase, its setting and stability, via temperature. As the fiber is heated it gets longer and thus the phase relative to the other fiber arms is shifted. For instance when we are scanning the temperature/phase in one interferometer we have a temperature dependence of around  $9\pi/K$ . Both interferometers are actively temperature stabilized and the interferometer that is left fixed is clearly stable over several periods as can be seen by the repeatability of the interference fringes inset in Fig.2. By looking at the interference fringes in the lateral peaks we can determine the relationship between the two free phases and hence we can vary them with a fixed, and known, relationship, e.g.  $\Phi_{jk}^R = r\Phi_{jk}^L$ , for some constant coefficient,  $r$ .

### 3. Characterization

So how can we characterize and quantify these states? From the perspective of the optician we would like to be able to define some interference fringe visibility to quantify the process. This can always be defined as  $V = (I_{max} - I_{min})/(I_{max} + I_{min})$  where, in the case of single photon detection, we can replace these maximum and minimum intensities with detection probabilities, with the limits taken over all possible phases. Before we determine the detection probabilities for these qutrit states we have defined we will introduce a standard, symmetric, noise model such that we can consider the case where we have,

$$\rho_{jk} = \lambda|\psi_{jk}\rangle\langle\psi_{jk}| + \frac{1-\lambda}{9}I_9. \quad (9)$$

With probability  $\lambda$  we expect our entangled qutrit state, and with probability  $(1-\lambda)$  we expect a maximally mixed state, at output  $jk$ . A symmetric model is assumed at the outset for its simplicity and due to the high degree of symmetry for the tritter coupling ratios. As we will see this theory fits very well with the experimental results and hence is justified.

If we do this we have the following probability for a coincidence detection projecting onto the mixed state of Eq.(9),

$$P_{jk} = \frac{1}{27} [3 + 2\lambda [\cos(\Phi_{jk}^R) + \cos(\Phi_{jk}^L) + \cos(\Phi_{jk}^R + \Phi_{jk}^L)]]. \quad (10)$$

We can clearly see the dependence of the phases associated with the right and left lateral peaks, as well as the sum of their values. From this we can derive quantities such as the fidelity and visibility.

The simplest phase relationship, and one that can lead theoretically to 100% visibility, demands that we maintain a constant relationship,  $\Phi_{jk}^R = \Phi_{jk}^L$ , as we scan the two phases.

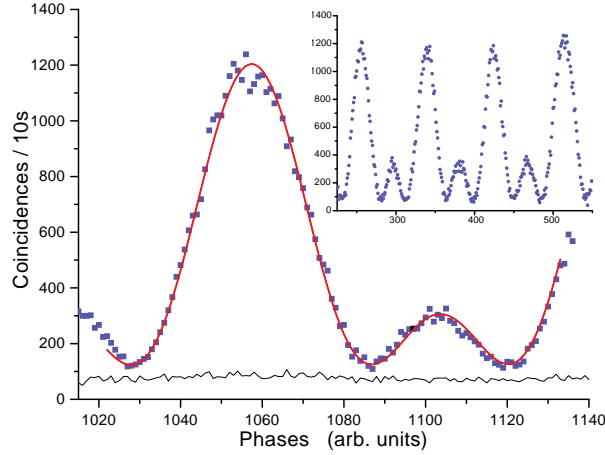


Fig. 2. Raw interference fringe, coincidence counts, for the central peak. The accidental coincidence (noise) level is also shown. Inset we see another interference pattern showing the stability and repeatability of the source.

A visibility of 100% can only be obtained for a discrete set of integer values for  $r$  which produce maximum destructive interference, that is, such that Eq.(10) goes to zero. In Fig.2 we see the coincidence count rate as the phases are scanned in this manner. The points are the experimental results and the solid line is a least-squares fit based on the function given in Eq.(10). We can also use this fit to find the maximum and minimum and hence also the visibility. Using this standard definition for the visibility we find both the net (noise subtracted) and raw values,  $V_{net} = 0.919 \pm 0.026$  and  $V_{raw} = 0.815 \pm 0.021$ . The noise consists of accidental coincidences due to detector noise and uncorrelated photons and is measured concurrently with the true coincidence counts. The noise level is shown just below the raw interference fringe in Fig.2. In the inset we have also shown a longer section of data illustrating the control and stability of this source.

It is clear from the form of Eq.(10) and Fig.2 that the interference fringes resulting from varying the two phases are qualitatively and quantitatively different from those of qubits which depend on just one sinusoidal function. One result of this is that we no longer have a simple relationship between fidelity and visibility that qubits provide. To obtain a qualitative relationship between these in the qutrit regime we need to satisfy very specific constraints for the two phases. Indeed if we take  $r = 1$  we can periodically scan through phase settings that determine projections onto three orthogonal maximally entangled qutrit states for  $\Phi_{jk}^R = \Phi_{jk}^L = \{0, 2\pi/3, 4\pi/3\}$ . If we do this then we can define the fidelity with respect to these maximally entangled qutrit states as  $F = \text{Tr}[\rho_{jk}\psi_{me}] = (1 + 8\lambda)/9$ . If we relax this phase constraint then the fit is parameterized by  $\lambda$  and the two phases. We find that the fit reveals a value of  $r = 1.027 \pm 0.003$  and then from the value for  $\lambda$  we can determine the fidelity of our source, with respect to these phases, using the definition previously stated. The results for both the net and raw Fidelity are  $F_{net} = 0.984 \pm 0.018$  and  $F_{raw} = 0.843 \pm 0.016$ . As expected the visibility is highly dependent on the relationship between the two phases however the source itself is capable of producing entangled qutrit states with a high degree of fidelity.

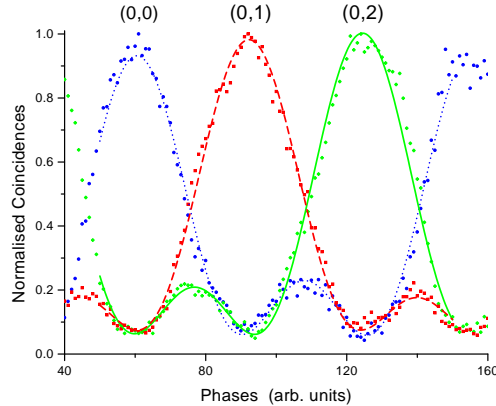


Fig. 3. Normalized interference fringes, as in Fig.2, for the three possible coincidence detections highlighting the three-fold symmetry.

In Fig.3 we see the normalized (accounting for variation in detection efficiency) coincidences and fits for all three coincidence outcomes measured at the same time. These all have the same form as that of Fig.2 and are equally distributed with respect to the phase axis. This separation corresponds to the  $t = 2\pi/3$  phase shift between the three possible outcomes. While we clearly see the 3-fold symmetry we also see that it is not perfect. The alignment between the minima and maxima changes slightly from one period to the next. This is due to the ratio between the two phases,  $r$ , not being exactly one.

#### 4. Conclusions

We have presented an experimental arrangement to generate, control and measure entangled qutrits. The system is readily adaptable to investigate both fundamental and applied aspects of high dimensional quantum systems, for example, entanglement and non-locality via Bell type inequalities as well as quantum key distribution. The results show a resource capable of producing high fidelity maximally entangled qutrits with good controllability ideal for quantum communication.

#### Acknowledgements

The Authors would like to acknowledge useful discussions with S. P. Kulik and his group through INTAS and the technical assistance of J-D.Gautier. This project is financed by the Swiss NCCR "Quantum Photonics" and the EU IST-FET project RamboQ.

#### References

1. M. A. Nielsen and I. L. Chuang, *Quantum Computation and Quantum Information*, Cambridge University Press, Cambridge, (2001).
2. N. Gisin *et al.*, *Rev. Mod. Phys.*, **74**, 145 (2002).
3. H. Bechmann-Pasquinucci and A. Peres, *Phys. Rev. Lett.* **85**, 3313 (2000).

4. N. J. Cerf, M. Bourennane, A. Karlsson and N. Gisin, Phys. Rev. Lett. **88**, 127902 (2002).
5. D. Bruß and C. Macchiavello, Phys. Rev. Lett. **88**, 127901 (2002).
6. M. Fitzi, N. Gisin and U. Maurer, Phys. Rev. Lett., **87** 217901 (2001).
7. A. Ambainis, Proc. STOC 01, 134 (2001).
8. C. A. Sackett *et al.*, Nature **404**, 256 (2000)
9. J. Pan *et al.*, Nature (London) **403**, 515 (2000).
10. T. Jennewein, G. Weihs, J. Pan and A. Zeilinger, Phys. Rev. Lett. **88**, 017903 (2002).
11. J. C. Howell, A. Lamas-Linares and D. Bouwmeester, Phys. Rev. Lett. **88**, 030401 (2002).
12. I. Marcikic *et al.*, Nature, **421**, 509 (2003).
13. A. V. Burlakov *et al.*, quant-ph/0207096 (2002).
14. A. Vaziri, G. Weihs, and A. Zeilinger , Phys. Rev. Lett. **89**, 240401 (2002).
15. H. de Riedmatten, I. Marcikic, H. Zbinden and N. Gisin, Quant. Inf. and Comp., **2** 6, 425 (2002).
16. J. D. Franson, Phys. Rev. Lett. **62**, 2205 (1989).
17. M. Reck, PhD-Thesis, University of Innsbruck, (1996)-  
<http://www.quantum.univie.ac.at/publications/thesis/index.html>.
18. G. Weihs, M. Reck, H. Weinfurter and A. Zeilinger, Opt. Lett. **21** 302 (1996).
19. G. Weihs, M. Reck, H. Weinfurter and A. Zeilinger, Phys. Rev. A **54**, 893 (1996).
20. S. Tanzilli *et al.*, Elect. Lett., **37**, 28 (2001).
21. M. Zukowski, A. Zeilinger and M. A. Horne, Phys. Rev. A **55**, 2564 (1997).
22. N. A. Peters *et al.*, quant-ph/0308003 (2003).
23. W. Tittel, J. Brendel, N. Gisin, and H. Zbinden, Phys. Rev. Lett **81**, 3656 (1999).
24. R. T. Thew *et al.*, Phys. Rev. A **66**, 062304 (2002).